Compositional variation and timing of aluminum phosphate-sulfate minerals in the basement rocks along the P2 fault and in association with the McArthur River uranium deposit, Athabasca Basin, Saskatchewan, Canada†

ERIN E. ADLAKHA[1,*] AND KEIKO HATTORI[1]

[1]Department of Earth Sciences, University of Ottawa, Ottawa, Ontario, K1N 6N5, Canada

ABSTRACT

The Athabasca Basin hosts world class uranium deposits, such as the McArthur River deposit. This paper presents the occurrence of aluminum phosphate-sulfate (APS) minerals in the metasedimentary rocks along the P2 fault, the main ore-hosting fault of the McArthur River deposit. It compares the APS minerals along the P2 fault with those outside the fault, examined in this study, and those from other deposits of the Athabasca Basin and from other Paleo- to Mesoproterozoic basins worldwide.

APS minerals are common along the P2 fault but rare outside of the P2 fault zone in the basement and along the unconformity between the Athabasca sandstones and the basement. The APS minerals along the P2 fault occur with sudoite (± illite, magnesiofoitite) and are zoned with Sr-, Ca-, and S-rich cores (solid solution between svanbergite, crandallite, and goyazite) and LREE- and P-rich rims (close to florencite composition). APS minerals in the Bleached Zone (altered rocks along the unconformity consisting predominantly of kaolin and illite) are Sr-, Ca-, and S-rich (high svanbergite component) and occur with kaolin. APS minerals in the Red-Green Zone (mingled red hematitic and green chloritic basement rocks below the Bleached Zone) occur with sudoite and clinochlore. They contain relict cores of LREE- and As-rich arsenoflorencite-(Ce) and rims of svanbergite-goyazite-crandallite solid solution.

The occurrence of svanbergite-crandallite-goyazite along the unconformity suggests their formation by relatively oxidizing fluids during diagenesis of the overlying sandstones. The relict cores of arsenoflorencite-(Ce) in the Red-Green Zone are interpreted to be the product of paleo-weathering before the deposition of the Athabasca sandstones. Florencitic APS minerals are found along the entire studied strike length (7 km) of the P2 fault, including the ore zone and non-mineralized areas, but are absent outside the fault zone. The florencitic APS minerals contain low SO_4^{2-} in the ore zone, suggesting relatively reducing conditions during their crystallization. Zoned APS minerals (with svanbergitic cores and florencitic rims) proximal to ore contain elevated U (up to 16 ppm). These features suggest that diagenetic, oxidizing, and uranium-bearing fluids traveled along the P2 fault and became relatively reduced, especially within the ore zone. It also suggests florencitic APS minerals are contemporaneous with uranium mineralization. The restricted occurrence of florencitic APS mineral along the P2 fault in the basement suggests their use in identifying fertile basement structures associated with uranium mineralization.

Keywords: Hydrothermal alteration, APS, uranium mineralization, florencite, svanbergite, arsenoflorencite, diagenesis, paleo-weathering, unconformity-type uranium deposits

INTRODUCTION

The Athabasca Basin hosts numerous large uranium deposits (Fig. 1), which are classified as unconformity-related uranium deposits. The prevalent model for mineralization was first proposed by Hoeve and Sibbald (1978) and modified later by many researchers (e.g., Alexandre et al. 2005; Derome et al. 2005; Richard et al. 2011; Mercadier et al. 2012). This model suggests that sea-water derived, uranium-bearing oxidizing brines (25–35 wt% eq. NaCl) precipitated uranium ore at the unconformity when it reacted with a reducing fluid of currently unknown origin. Many deposits occur in the proximity of deformation zones in the basement and it is suggested that re-activated basement faults served as conduits for uranium-bearing fluids (Jefferson et al. 2007) or reducing basement fluids to reach the unconformity (McGill et al. 1993). The McArthur River deposit, the largest discovered high-grade (average grade of 16.46% U_3O_8; Bronkhorst et al. 2012) uranium deposit on Earth, is situated along the P2 fault, a 13 km long reverse fault constrained to graphitic metapelite below the Athabasca Basin. Although geophysical and structural studies have been carried out on the P2 fault (e.g., Hajnal et al. 2010), the exact role of the fault in the mineralization remains uncertain.

In the Athabasca and Thelon basins of Canada, aluminum phosphate-sulfate (APS) minerals (also known as aluminophosphate sulfate) spatially associated with uranium deposits have been reported (Quirt et al. 1991; Gall and Donaldson 2006;
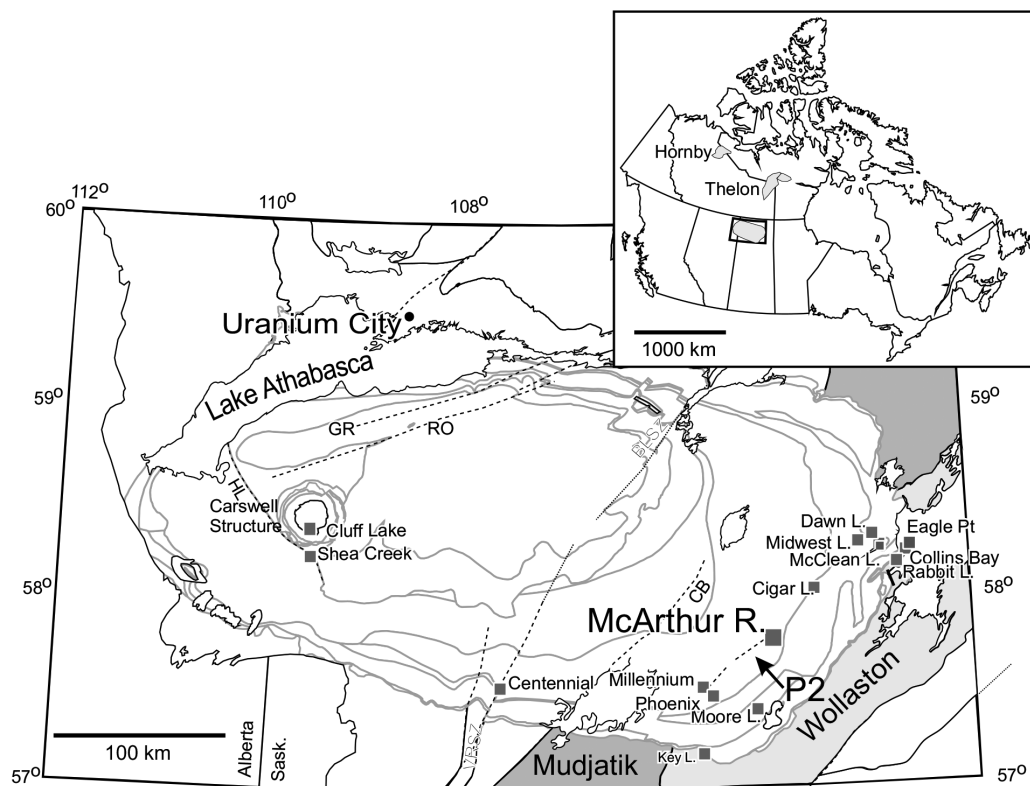
FIGURE 1. A map showing the location of the major uranium deposits (squares), including McArthur River deposit, and basement structures (dashed lines), including the P2 fault, in the Athabasca Basin (modified from Jefferson et al. 2007). The southeastern margin of the Athabasca Basin is underlain by the basement rocks of the Wollaston and Mudjatik Domains of the western Churchill Province. An insert shows the locations of the Athabasca basin relative to other two Mesoproterozoic sedimentary basins: Hornby and Thelon basins. Major shear zones: BB = Black Bay, BLSZ = Black Lake Shear Zone, CB = Cable Bay, GR = Grease River Shear Zone, RO = Robbilard, VRSZ = Virgin River Shear Zone.

Gaboreau et al. 2007; Riegler et al. 2014). APS minerals occur in various environments (Dill 2001) and form many solid-solution series with over 40 end-members (Jambor 1999; Stoffregen et al. 2000; Dill 2001). APS minerals have the general formula: $AB_3(XO_4)_2(OH)_6$, where A = mono-, di-, tri- or, more rarely, tetravalent cations (K^+, Na^+, Rb^+, Ca^{2+}, Sr^{2+}, REE^{3+}, Th^{4+} etc.); B = trivalent cations (Al^{3+}, Fe^{3+}); and X = P^{5+}, S^{6+}, or As^{5+}. Since the incorporation of ions with different valences requires coupled substitution to accommodate charge balance, compositional zoning of APS minerals is commonly well preserved. This makes APS minerals excellent candidates for evaluating the chemical and physical characteristics of fluids from which they formed (Dill 2001; Beaufort et al. 2005; Gaboreau et al. 2005, 2007).

The focus of this paper is to present the occurrence and compositional variation of APS minerals in basement rocks along the P2 fault, discuss the role of the fault during mineralization and the timing of APS mineral formation with respect to uranium mineralization. In addition, the chemistry of APS minerals is compared with those along and outside of the fault zone in the basement, from other APS minerals studied in Athabasca Basin (within deposits or not), and from other Paleo- to Mesoproterozoic basins worldwide. The potential use of APS minerals in exploration for unconformity-related uranium deposits is also discussed.

GEOLOGICAL SETTING

Regional geology

The basement rocks in the eastern Athabasca Basin area are part of the Wollaston and Mudjatik Domains. The rocks of the Wollaston Domain consist of metapelite, metasemipelite, meta-arkose, calc-silicate, and quartzite (e.g., Annesley et al. 2005). They were metamorphosed under upper amphibolite to lower granulite conditions during the Trans-Hudson Orogeny (ca. 1.8–1.9 Ga; Lewry and Sibbald 1980; McKechnie et al. 2012). Abundant granitic pegmatite lenses intruded the metasedimentary rocks during peak metamorphism (Annesley et al. 2005; Jefferson et al. 2007).

Alteration immediately below the unconformity is laterally extensive and consists of a deeper Green Zone with sudoite (Al-Mg chlorite) and illite ± Fe-Mg chlorite, a transitional Red-Green Zone with illite, sudoite, and hematite, an upper Red Zone with hematite and kaolin ± illite, and, locally, there is Bleached Zone of kaolin and illite, immediately beneath the unconformity (Macdonald 1985; Quirt 2001; Adlakha et al. 2014). In addition to the Red-Green transitional Zone, the Red and Green Zones are mingled in places. The origin of these Zones has been in discussion. Macdonald (1985) considered them as the products of paleo-weathering before sandstone deposition, whereas Cuney et al. (2003) proposed their formation after the deposition of sandstones. Quirt (2001) and

Adlakha et al. (2014) pointed out extensive overprinting of alteration minerals by subsequent hydrothermal fluids, which makes it difficult to determine the condition of their initial crystallization. Rocks of the Bleached Zone are altered to white due to loss of hematite and interpreted to be a reaction product of the Red Zone with late diagenetic fluids from the overlying basin (Macdonald 1985; Quirt 2001). The least-altered metapelite occurs >50 m below the unconformity and away from faults.

The sedimentary rocks of the Athabasca Group are comprised of dominantly fluvial to shallow marine, quartz pebble conglomerate and quartz arenite, with a preserved maximum thickness of 1500 m in the center of the basin (Ramaekers et al. 2007). Early diagenesis included silica cementation on hematite-dusted detrital quartz grains (Hoeve and Quirt 1984; Jefferson et al. 2007), alteration of kaolinite by dickite with minor illite and locally traces of sudoite (Quirt 2001; Laverret et al. 2006). Uranium deposits are localized near the intersection of the unconformity and basement faults or down-dip along these faults into the basement. These

deposits are surrounded by alteration haloes of sudoite, illite, and magnesio-foitite (alkali-deficient dravite). Sandstone-hosted unconformity-type deposits show the inner halo of sudoite with an outer alteration halo of illite (e.g., Hoeve et al. 1981; Hoeve and Quirt 1984; Alexandre et al. 2012). Basement-hosted unconformity-type deposits are accompanied by the inner alteration halo of illite and the outer halo of sudoite. The different proportions of sudoite and illite between two types of unconformity-type deposits are considered to be related to differences in fluid circulation (i.e., Ingress vs. Egress; Hoeve and Quirt 1984).

Structure and alteration of the McArthur River deposit and P2 fault

The McArthur River deposit is comprised of six ore bodies, Zones 1–4 and Zones A and B, which collectively have a strike length of approximately 1.7 km near the intersection of the P2 fault (~050°/45–60°) and the unconformity, ~500 m below surface (Fig. 2) (McGill et al. 1993; Alexandre et al. 2005;
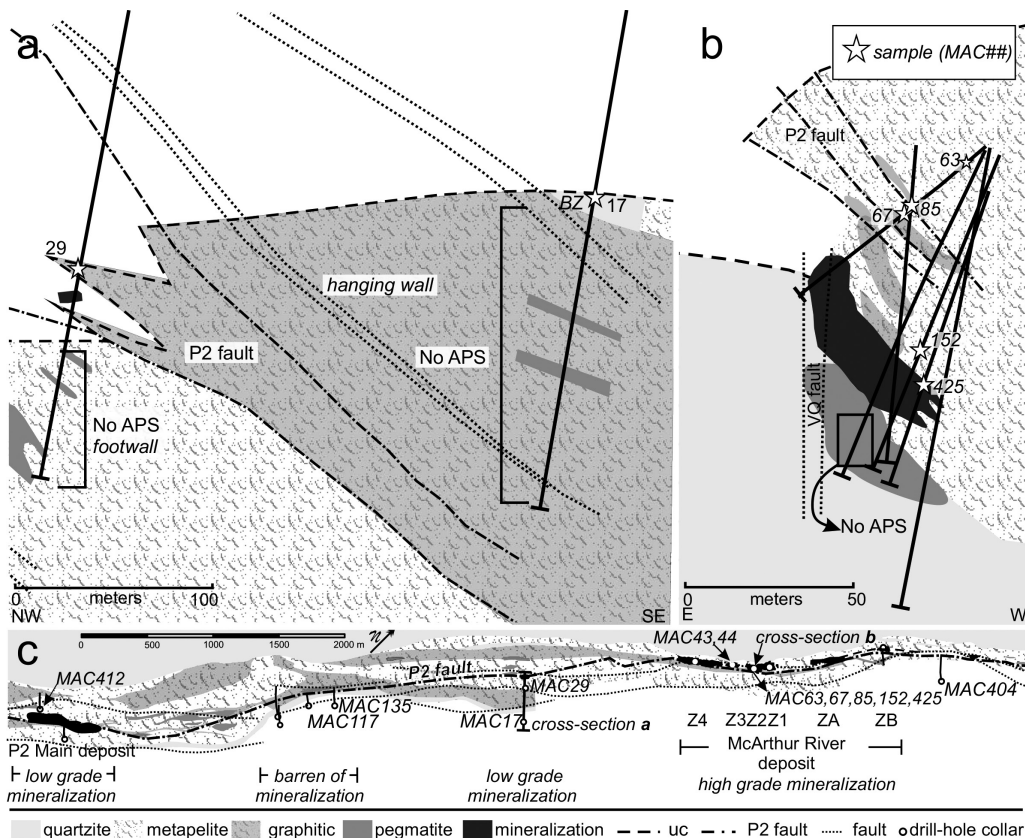
FIGURE 2. Schematic cross sections (**a**, **b**) showing the distribution of APS minerals and sample locations (stars), and a geologic map (**c**) at the unconformity showing drill-hole locations. (**a**) APS minerals are found in the P2 fault proximal to low-grade mineralization (sample MAC29) and in the Bleached Zone (BZ) in quartzite (sample MAC17); (**b**) APS minerals are found in the P2 fault proximal to the Zone 2 ore body (samples MAC63, 67, 85, 152, 425). APS minerals were not found in samples from the footwall and hanging-wall (indicated "No APS") nor in samples collected from the VQ fault. (**c**) An interpreted geological strip map at the unconformity showing the P2 fault, the locations of sampled drill-holes and ore bodies, sample locations, and the sites of the cross sections (**a**, **b**). The P2 fault is essentially barren in the southwestern part. Low-grade mineralization occurs along the middle and southeast (P2 Main deposit) portions of the P2 fault. APS minerals were found in one sample (sample MAC412) of the Red-Green Zone in the footwall proximal to the P2 Main mineralization. Z1–4 = Zone numbers of ore body at the McArthur River deposit; uc = unconformity. Cross sections and map were modified from Cameco internal reports.

Bronkhorst et al. 2012). The total reserves of the McArthur River deposit as of August 31, 2012, were 385.5 Mlbs U_3O_8 (Bronkhorst et al. 2012). All ore bodies are hosted in the sandstone immediately above the unconformity except for the Zone 2 ore body, which occurs immediately below the unconformity and is bounded by the vertical quartzite (VQ) fault and ~140° trending series of cross faults (Fig. 2b). Late minor remobilizations of uraninite formed veinlets and fractures with pyrite, chalcopyrite, and minor nickel-cobalt sulfarsenides (McGill et al. 1993).

The P2 fault zone is a series of reverse faults with a strike length of approximately 13 km (McGill et al. 1993) and has been traced seismically at least 2 km below the unconformity (Hajnal et al. 2010). In the basement, the several fault planes of the P2 fault are mostly constrained to graphite-bearing metapelite and trend parallel to the basement foliation (McGill et al. 1993). Reactivation of P2 faulting formed differences in the thickness of the basal conglomerate at the unconformity and broad fracture and breccia zones in the sandstones. The reverse movement of the P2 fault raised a wedge of basement rocks above the unconformity with the vertical displacement of up to 80 m (McGill et al. 1993; Figs. 2a and 2b). The basement wedge is also referred to as the "middle block" by workers (Bronkhorst et al. 2012) as it is offset by differential movement of fault planes (Figs. 2a and 2b). These offsets commonly host the uranium mineralization of McArthur River deposit and sporadic occurrences of low-grade (<1% U_3O_8) mineralization along the P2 fault (Fig. 2a). The P2 fault and basement rocks show minor lateral displacement by three sets of steeply dipping faults that strike 100–110° in the mine-site area (Fig. 2b). These faults and offsets likely provided pathways for mineralizing fluids, but also truncate high-grade zones, especially the Zone 2 ore body (Fig. 2b; McGill et al. 1993; Bronkhorst et al. 2012).

Basement rocks along the P2 fault were intensely altered to form sudoite, illite, magnesio-foitite, Fe-Mg chlorite, and sulfides (McGill et al. 1993; Adlakha et al. 2014). The hanging wall basements rocks, including the ore-hosting wedge, commonly show intense alteration forming sudoite and illite ± kaolin. The alteration forming illite and/or kaolin gives the rocks a creamy white color, and this alteration is called "bleaching". Bleaching is common, especially in close proximity to the fault, mineralization, and the unconformity (McGill et al. 1993). The most intense alteration of the basement rocks is found in close proximity to the Zone 2 ore body where sudoite and magnesiofoitite are the dominate alteration minerals (Adlakha et al. 2014). In comparison, illite with minor sudoite are the dominate alteration minerals in the moderately altered basement rocks in unmineralized areas (the southwest portion of the P2 fault) and near the weakly mineralized P2 Main deposit (Fig. 2b), that is "perched" higher in sandstones. APS minerals only occur in highly altered rocks where primary metamorphic minerals and textures are altered.

Sampling

A total of 192 samples of metasedimentary rocks, predominately metapelites with fewer pegmatite and quartzite, were collected from 27 different drill-holes along, and within proximity to, the P2 fault zone from the McArthur River mine site to ~7 km southwest (Fig. 2c). Of these, 139 samples were selected for examination of APS minerals in thin sections. Out of the 139

samples, APS minerals were found in only 17 samples. Among these 17 samples, APS minerals in 4 samples were too small for quantitative analysis with electron microprobe analyzer (EPMA). Of these remaining 13 samples (Table 1), nearly all were from metapelites located along the P2 fault (11 of 13) that showed intense/pervasive alteration in which clay-sized minerals replaced most metamorphic minerals and metamorphic textures were obliterated by alteration, fractures and/or veinings. In this paper, samples collected within 50 m of the center of the fault are considered to be associated with P2 fault, as the fault is accompanied by splay structures and alteration extending outside the fault zone.

The samples associated with the P2 fault were collected from varying distances to the McArthur River uranium deposit (Fig. 2c; Table 1). MAC425 was collected within the Zone 2 ore body (Fig. 3a), MAC152 <15 m from the Zone 2 ore body, MAC67 (Fig. 3b) and MAC85 <20 m from the Zone 2 ore body, MAC63 <50 m from the Zone 2 ore body, MAC43 and MAC44 <50 m from the Zone 3 ore body. MAC29 was within 1 m of low grade (<1 wt% U_3O_8) uranium mineralization disseminated within the sandstone (Fig. 2a), MAC404 was approximately 50 m from low grade uranium mineralization within the sandstone. MAC117 and MAC35 are >500 m away from low-grade uranium mineralization in the sandstone, >1 km from the low-grade P2 Main deposit, and >2 km from the McArthur River deposit.

Although 5 samples from the Bleached Zone were examined in detail, APS minerals were found only in one sample (MAC17; Fig. 3c) of quartzite along the unconformity, >250 m from low-grade mineralization and >1 km from the McArthur River deposit (Figs. 2a and 2c). Twenty-two samples of metasedimentary rocks of the Green, Red-Green, and Red Zones outside the P2 fault were examined and APS minerals were found only in one sample (MAC412) of strongly hematized and chloritized metapelite from the Red-Green Zone in the footwall near the P2 Main deposit (Figs. 2c and 3d). Here we use field terminology "Bleached Zone" and the "Red-Green Zone" to reflect the samples position within the basement rocks as these terms were commonly used by geologists in the area. The Bleached Zone occurs along the unconformity and it refers to a creamy-white colored zone where kaolin and illite predominate. The Red-Green Zone is a physical mixture of hematitic Red Zone and chloritic Green Zone.

METHOD

Thin sections were examined using an optical petrographic microscope with reflected and transmitted light sources. Due to the very fine-grained nature of minerals in the samples, detailed textural analysis was also carried out on carbon-coated polished thin sections using a JEOL 6610LV scanning electron microscope (SEM) at the University of Ottawa. Minerals were identified using energy-dispersive spectroscopy with the spectrum acquisition time of 40 s and an accelerating voltage of 20 kV.

Quantitative analysis for the major and minor elemental compositions of the APS minerals was carried out using a JEOL 8230 EMPA at the University of Ottawa. APS minerals were analyzed at an accelerating voltage of 15 kV, a beam current of 20 nA using a focused beam of 5 μm (to account for alkali migration). Counting times were 20 s on-peak and 10 s off-peak for all elements except for S (10 s on and 5 s off), F (50 s on and 25 s off), Pr (20 s on and 5 s off) Cl (25 s on 12 s off), P (10 s on and 5 s off), Si (10 s on and 5 s off) and As (20 s on and 20 s off). The mineral standards used were sanidine (Si, Al, K), hematite (Fe), apatite (Ca, P, F), albite (Na), tugtupite (Cl), celestine (Sr, S), synthetic $NdPO_4$ (Nd), $PrPO_4$ (Pr), $CePO_4$ (Ce), $LaPO_4$ (La), ThO_2 (Th), and GaAs (As). The elemental concentrations were calculated after matrix interference correction using ZAF. Elemental maps of selected APS grains were acquired at an accelerating voltage of 10 kV with a 10 nA current at a counting time of 0.5 s per pixel with a total of 10000 pixels per image.

TABLE 1. Sample descriptions

DDH[b]	Sample	Depth[c]	Proximity to P2 fault[d]	Proximity to uc[d]	Proximity to U-min[d]	Degree of alteration and rock-type[d]
				P2[a]		
MC370	MAC29	560.2	in the P2 fault zone	u/c (Fig. 2A)	<1 m from lg U-min in ss	moderately altered mp
H729	MAC43	49.5	in the P2 fault zone	~15 m	<50 m from Z3 ore	green intensely altered graphitic mp
H729	MAC44	64.5	~15 m laterally from P2 in fw	~15 m	<50 m from Z3 ore	red and white intensely altered peg
H201	MAC63	7.6	~30 m laterally from P2 in hw	~20 m	<50 m from Z2 ore	green intensely altered mp
H201	MAC67	30.8	the P2 fault zone	~20 m	<20 m from Z2 ore	green intensely altered peg
H493	MAC85	17.7	in the P2 fault zone	~20 m	<20 m from Z2 ore	intensely altered graphitic mp w/ peg boudins
H203	MAC152	62	in the P2 fault zone	~50 m	<15 m from Z2 ore	green-white intensely altered mp
MC410	MAC404	542.7	~50 m laterally from P2 in hw	~15 m	~50 m laterally from lg in ss	red moderately altered mp w/ peg boudins
H3380	MAC425	57.1	in the P2 fault zone	~50 m	Z2 ore	green intensely altered mp with U-ore
MC361	MAC117	523.3	in the P2 fault zone	~25 m	>500 m from U-min	white-green intensely altered peg
MC362	MAC135	520.2	~40 m above P2 in hw	~10 m	>500 m from U-min	red-green intensely altered peg
				RGZ		
MC346	MAC412	669	~100 m laterally from P2	~50 m	~100 m below P2 Main	red-green intensely altered mp
				BZ[a]		
MC344	MAC17	499.4	~250 m laterally from P2 in hw	<1 m	>250 m from U-min	quartzite with bleached matrix

[a] P2 = P2 fault sample; RGZ = Red-Green Zone sample; BZ = Bleached Zone sample.
[b] DDH = diamond drill-hole number.
[c] Drill-hole with the prefix H are collared underground, therefore sample depths are not from the surface.
[d] U-min = uranium mineralization in the McArthur River deposit; fw = footwall; hw = hangingwall; lg = low-grade (<1 wt% U_3O_8); ss = sandstone; uc = unconformity; peg = pegmatite; mp = metapelite.
[e] Ap = apatite; Clc = clinochlore; Dck = dickite; Drv = dravite; Fe-Mg chl = Fe-Mg chlorite; fg = fine-grained; Gr = graphite; Ilt = illite; Mgf = magnesiofoitite, Py = pyrite; Qz = quartz; Rt = rutile; sud = sudoite; U = uraninite; xtm = xenotime; zrn = zircon.   *(Table extends on next page.)*

APS minerals are small (mostly <20 μm, rarely up to 40 μm) and surrounded by quartz and fine-grained alteration minerals (Fig. 4; Tables 1–2), but it was necessary to use a broad electron beam of 5 μm to minimize the loss of alkalis from APS minerals during the EPMA analysis. This made it unavoidable for the surrounding minerals to contribute to the analytical results. To evaluate the possible contributions of surrounding minerals in the chemical composition obtained for the APS, their compositions were measured by EMPA. The contents of SiO_2 were used to monitor the contribution of surrounding minerals because APS minerals rarely contain Si. For the data showing Si, the amounts of K, Al, and Na of the surrounding phases were subtracted from the analytical results. For example, for Al_2O_3 using the equation, $Al_2O_{3APS\ corrected} = Al_2O_{3APS\ analyzed} - (SiO_{2APS\ analyzed} \cdot Al_2O_{3matrix}/SiO_{2matrix})$. The remaining concentration values were normalized to the original analytical total. Table 2 shows the contents of SiO_2 before subtracting the contribution of surrounding minerals. The contribution of surrounding minerals never exceeded 5% of the total.

Trace element contents in the APS minerals were determined using polished thick (>60 μm) sections by laser ablation-inductively coupled plasma-mass spectrometer (LA-ICP-MS) at the Geological Survey of Canada, Ottawa, using a Photon-Machines Analyte193 ArF excimer laser (λ = 193 μm) with Helex ablation cell and Agilent

7700x quadrupole ICP-MS. Helium gas was used to transport ablated sample from the ablation cell and was mixed with Ar plasma (flow rate of 1.05 mL/min) via a T-connector before entering the ICP. The detailed operating conditions for the LA-ICP-MS instrument and the isotopes quantified are listed in Appendix Table 1[1]. During analysis, ~40 s of background signal with the laser turned off was collected and then ablation was performed by a laser focused to 10 μm for a data acquisition time of ~60 s (total time of 100 s for one analysis) for a total time of 100 s for one analytical cycle. The isotope counts were monitored during the analysis and the acquisition time for the data of APS minerals was adjusted (Appendix Fig. 1[1]). Aluminum contents are similar among grains of APS minerals and Al does not vary between the core and rim of APS minerals (Table 2). Therefore, the elemental concentrations were obtained based on the count ratios of elements to the average Al in the sample (determined by EMPA; Table 2), and the reference NIST610 (National Institute of Standards and

[1] Deposit item AM-15-75069, Supplementary tables and figures. Deposit items are stored on the MSA web site and available via the *American Mineralogist* Table of Contents. Find the article in the table of contents at GSW (ammin.geoscienceworld.org) or MSA (www.minsocam.org), and then click on the deposit link.

FIGURE 3. Photographs of selected drill-core samples; (**a**) uranium ore of the Zone 2 ore body and P2 fault (MAC425); (**b**) intensely sudoite-altered pegmatite from the P2 fault (MAC67); (**c**) quartzite from the Beached Zone along the unconformity (MAC17); and (**d**) hematitized and chloritized metapelite from the Red-Green Zone (MAC412). Sample locations are shown in Figure 2. (Color online.)

TABLE 1.—*Extended*

APS occurrence	Clay[e]	Mineralogy[f]
Zone P2[a]		
isolated, 3–10 µm	Sud	Mgf, Xtm, Qz
isolated, 3–10 µm	Sud/Ilt	Mgf, Gr, Py, Ap, Zrn, Xtm
zoned, clustered, 5–20 µm	Sud/Ilt	Hem, Mnz, Zrn, Qz, Gr, Py
zoned, clustered, fragmented, 1–20 µm	Sud	Ilt, Rt, Ap, Fe-Mg Chl, Ilt, Py, Qz
zoned, clustered, 5–20 µm	Sud	Mgf, Ilt, Py, Ap, Qz
zoned, disseminated, 5–20 µm	Sud/Ilt	Drv, Py
zoned, disseminated, 5–30 µm	Sud/Clc	Mgf, Ill, Py, Qz, Ccp
disseminated, <1 µm	Kln	Hem, Ap
some cores missing, isolated, 3–10 µm	Mgf/Sud/Ilt	U, Hem
isolated, 3–10 µm	Ilt	Fe-Mg Chl, fg Qz, Qtz
disseminated, <1 µm	Ilt	Hem, Rt, fg Qz
Zone RGZ		
large clusters up to 0.5 mm, 10–40 µm	Sud/Clc	Hem
Zone BZ[a]		
disseminated, <1 µm	Kln	Ilt, Zrn, Qz

▼**Figure 4.** Photomicrographs (**a**, **b**, **f**) and SEM BSE (**c–e**, **g–l**) images of APS minerals. (**a**) Disseminated APS grains in fine-grained illite (Ilt) and with hematite (Hem); (**b**) clustered APS grains in contact with an aggregate of feather-textured, magnesiofoitite (Mgf) and a mixture of sudoite+illite+magnesiofoitite (Sud/Ilt/Mgf); (**c**) zoned APS grains in magnesiofoitite; (**d**) oscillatory-zoned APS crystals disseminated in a mixture of clinochlore+illite+magnesiofoitite (Clc-Ilt-Mgf) with chalcopyrite (Ccp); (**e**) zoned APS crystals clustered in magnesiofoitite+sudoite; (**f**) zoned APS crystals, apatite, and magnesiofoitite in a mixture of sudoite+illite; (**g**) partially corroded zircon (Zrn) mantled by xenotime (Xtm) and APS grains; (**h**) aggregate of euhedral, zoned APS crystals in a clinochlore+sudoite matrix; (**i**) disseminated, sub-hedral APS grains in fine-grained kaolin (Kln); (**j**) a mixture of APS minerals and quartz rimming coarse quartz grain; (**k**) APS grain in contact with pyrite (Py); (**l**) APS crystal with inclusions of Fe-oxide in contact with apatite (Ap). Sample number and location are indicated at the bottom left corner of each image. Qz = Quartz. (Color online.)
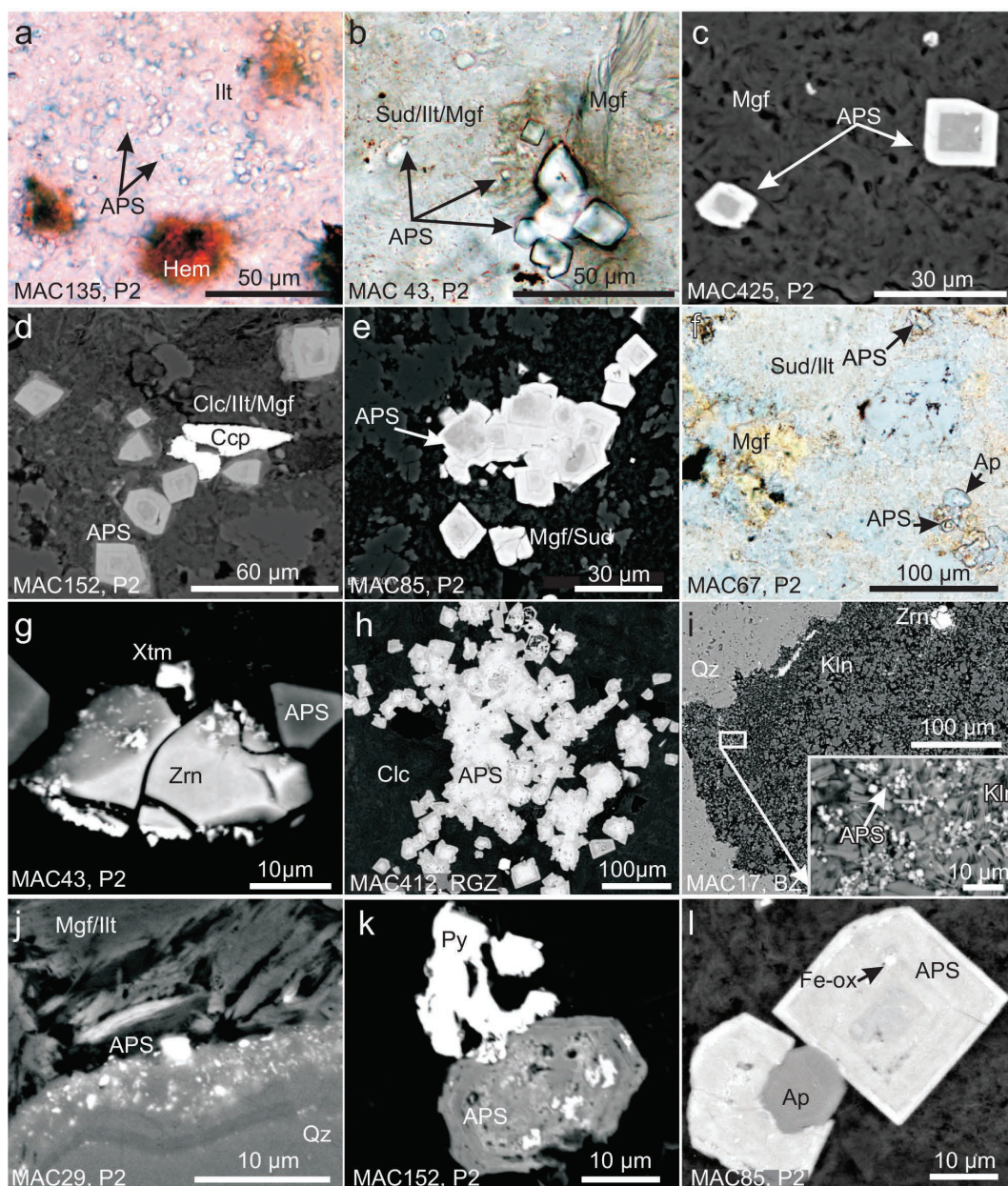
TABLE 2. EMPA major element oxide data and atomic proportion formula units for APS minerals

							P2 fault									
Sample a	MAC67		MAC85		MAC152						MAC404		MAC117		MAC425	
	Sud		Sud/Ilt		Sud/Clc						Kln		Ilt		Mgf/Sud	
b	Mixed		Mixed		Mixed		Core		Rim		Mixed		Mixed		Mixed	
No. grains	10	1σ	11	1σ	8	1σ	3	1σ	3	1σ	10	1σ	10	1σ	9	1σ
CaO	2.72	0.30	2.70	0.36	2.86	0.44	2.92	0.24	2.37	0.31	3.40	0.18	2.68	0.36	2.79	0.67
SO_3	1.68	0.77	1.69	1.29	2.06	0.53	2.58	0.44	1.14	0.30	0.94	0.37	3.70	0.46	3.43	1.48
Al_2O_3	28.96	1.56	31.26	1.30	32.01	1.08	32.30	0.31	31.26	0.63	31.13	1.25	32.22	1.07	32.37	1.10
Fe_2O_3	0.85	0.77	0.54	0.51	0.54	0.24	0.58	0.24	0.44	0.05	0.91	0.63	0.82	0.71	0.96	0.57
Nd_2O_3	3.26	0.44	3.29	0.79	2.77	0.50	2.44	0.33	3.80	0.47	4.26	0.37	2.16	0.42	2.20	0.36
Pr_2O_3	0.94	0.16	0.87	0.23	0.76	0.21	0.75	0.08	0.97	0.08	0.96	0.06	0.60	0.12	0.70	0.15
Ce_2O_3	8.67	1.21	8.33	1.09	7.81	0.78	7.74	0.37	9.44	0.54	7.50	0.48	7.85	0.80	7.50	1.78
La_2O_3	5.40	0.82	5.55	0.31	5.18	0.47	5.11	0.29	5.33	0.42	3.58	0.19	5.58	0.87	4.50	1.22
P_2O_5	25.84	1.71	26.76	1.17	27.10	0.58	26.66	0.64	28.20	0.27	28.85	1.43	25.24	0.73	25.71	1.17
SrO	3.14	0.64	3.17	1.08	3.73	0.62	4.09	0.37	2.64	0.25	3.65	0.74	4.38	0.45	5.49	1.64
ThO_2	0.51	0.29	0.27	0.38	0.16	0.05	0.15	0.09	0.11	0.07	0.15	0.10	0.04	0.02	0.13	0.09
As_2O_5	0.02	0.01	0.02	0.02	0.01	0.01	0.01	0.01	0.01	0.01	0.06	0.05	0.04	0.01	0.01	0.02
Total	81.98	2.61	84.46	1.99	84.98	0.92	85.34	0.96	85.70	0.76	85.40	0.89	0.04	1.40	85.78	1.45
SiO_2 c	*1.44*	*1.54*	*0.63*	*0.30*	*0.39*	*0.10*	*0.41*	*0.12*	*0.36*	*0.29*	*5.85*	*4.21*	*1.19*	*0.77*	*1.88*	*1.44*
apfu																
Ca	0.25		0.24		0.25		0.25		0.21		0.29		0.23		0.24	
Sr	0.16		0.16		0.17		0.19		0.13		0.17		0.21		0.25	
Nd	0.10		0.10		0.08		0.07		0.11		0.12		0.06		0.06	
Pr	0.03		0.03		0.02		0.02		0.03		0.03		0.02		0.02	
Ce	0.27		0.25		0.23		0.23		0.28		0.22		0.23		0.22	
La	0.17		0.17		0.16		0.15		0.16		0.11		0.17		0.13	
Fe^{3+}			0.03		0.03		0.04		0.03		0.02		0.05		0.06	
Al			0.05		0.06		0.07		0.02				0.07			
Th	0.01															
A	**1.00**		**1.02**		**1.00**		**1.02**		**0.97**		**0.97**		**1.04**		**0.99**	
Al	2.95		3.00		3.00		3.00		3.00		2.96		3.00		3.06	
Fe^{3+}	0.06										0.04		0.00		0.00	
B	**3.01**		**3.00**		**3.00**		**3.00**		**3.00**		**3.00**		**3.00**		**3.06**	
P	1.89		1.87		1.86		1.82		1.96		1.97		1.73		1.75	
S	0.11		0.10		0.12		0.16		0.07		0.06		0.23		0.21	
As																
X	**2.00**		**1.97**		**1.98**		**1.98**		**2.03**		**2.03**		**1.96**		**1.95**	
ΣLREE	0.58		0.54		0.51		0.47		0.58		0.48		0.48		0.44	
Ce anomaly d	0.83		0.81		0.85		0.85		0.89		0.87		0.92		0.90	
S/P e	0.06		0.05		0.06		0.06		0.04		0.03		0.13		0.12	

a Adjacent minerals, Ilt = illite, Sud = sudoite, Mgf = magnesiofoitite; Clc = clinochlore.
b Area of analysis in grains, i.e., rim, core, or mixed. Compositional zones are narrower than the beam size of 5 μm. The mixed area refers to the data from different compositional zones defined in SEM-BSE images.
c Contribution of surrounding minerals in the analytical data was evaluated using SiO_2 contents (see the Results for detailed description).
d $[Ce]_N{}^* = \sqrt{([La]_N \cdot [Pr]_N)}$.
e Atomic ratio of S to P.   *(Table extends on next page.)*

Technology) (Longerich et al. 1996). The average Al content was used as the same grains could not be analyzed both by EPMA and LA-ICP-MS because the electron beam decomposes APS minerals (Appendix Fig. 2[1]). EMPA and LA-ICP-MS data are comparable (Appendix Fig. 3[1]). There is no international standard that has the composition similar to APS minerals. Therefore, the standard NIST610 was used as it contains high Al and it is the most used standard. One round of LA-ICPMS analysis consisted of seven analyses of grains, bracketed by two analyses of the NIST610 reference and one analysis of the BCR2G (Basalt, Columbia River) reference from USGS. The analysis of NIST610 shows that a counting precision of >98% for all elements. Accuracy, determined by BCR2G, was >90% for all elements except for Sc, Ti, Fe, Zn, Ce, Pr, Sm, Ho, Lu, Gd, Tb, Pb, and Th, which were >85% and Cu, Y, Zr, Cr, Tm, Yb, and Hf that were >75%.

RESULTS

Mineral occurrence and distribution

APS minerals were found along the entire 7 km section of the P2 fault examined (Fig. 2). APS minerals were found only in one sample from the Bleached Zone (sample MAC17 in quartzite) (Figs. 2a, 3c, and 4i; Table 1). APS minerals are rare in the basement rocks distal from the unconformity and outside the P2 fault. They were found in only one sample (sample MAC 412) of the Red-Green Zone in the footwall 100 m from the P2 fault, 50 m below the unconformity and 100 m away from uranium mineralization (Figs. 3d and 4h; Table 1). APS minerals were not observed in samples along the VQ fault (Fig. 2b) or in samples of the least-altered basement rocks.

APS minerals along the P2 fault occur together with fine-grained sudoite and/or illite intergrown with magnesiofoitite (Adlakha et al. 2014; Figs. 4a–4f). In the Bleached Zone sample, APS minerals occur with kaolin and illite (Fig. 4i). APS minerals in the transitional Red-Green Zone occur predominately with clinochlore (Fig. 4h).

APS minerals are small (mostly <20 μm, rarely up to 40 μm), transparent, pseudo-cubic (rarely hexagonal) crystals, disseminated and/or clustered in fine-grained clay minerals (Fig. 4). There is no evidence of dissolution between APS minerals and surrounding clay minerals. The texture suggest that they are in equilibrium (Figs. 4a, 4j, 4l). APS minerals are commonly zoned. Zoning may be observed using plane polarized light microscopy as some cores show high relief. SEM BSE images commonly show darker cores with lighter rims (Fig. 4c), although grains with lighter cores and darker rims are also observed (Fig. 4h). Darker parts in BSE images are due to greater amounts of Sr and Ca, and

TABLE 2.—*Extended*

	P2 fault										RGZ					BZ	
Sample	MAC135		MAC63		MAC29		MAC44		MAC43		MAC412					MAC17	
a	Ilt		Sud		Sud		Sud/Ilt		Sud/Ilt				Sud/Clc			Kln	
b	Mixed		Mixed		Mixed		Mixed		Mixed		Mixed		Core		Rim	Mixed	
No. grains	3	1σ	7	1σ	4	1σ	14	1σ	2	1σ	10	1σ	2	1σ	2	1σ	3	1σ
CaO	3.14	0.11	3.34	0.31	1.95	0.26	3.18	0.19	2.98	0.45	3.49	0.36	3.46	0.42	3.87	0.44	1.76	0.19
SO_3	3.40	0.28	4.49	0.35	3.14	0.83	4.80	0.51	5.86	1.33	2.84	0.24	2.89	0.17	3.27	0.53	8.41	0.85
Al_2O_3	29.49	0.98	32.82	0.64	30.28	1.90	32.52	0.78	31.99	0.46	30.15	1.01	28.78	0.65	31.57	1.76	29.33	0.90
Fe_2O_3	1.40	0.56	0.23	0.11	1.90	0.87	0.50	0.19	0.31	0.14	3.49	1.66	5.85	2.02	3.37	2.99	0.34	0.11
Nd_2O_3	1.41	0.17	2.79	0.54	2.62	0.33	1.84	0.19	2.26	0.37	0.68	0.26	0.74	0.02	0.48	0.23	1.21	0.32
Pr_2O_3	0.50	0.12	0.71	0.16	0.76	0.09	0.58	0.17	0.46	0.17	0.12	0.09	0.25	0.08	0.19	0.07	0.31	0.25
Ce_2O_3	8.81	0.63	6.75	0.46	4.65	0.70	6.07	0.70	5.84	0.44	11.16	0.80	9.40	1.05	10.19	1.26	1.71	0.64
La_2O_3	2.83	0.27	3.78	1.01	4.08	1.33	3.95	0.47	3.28	0.25	1.32	0.39	1.56	0.52	1.26	0.74	1.01	0.36
P_2O_5	26.65	0.66	25.52	0.63	23.95	0.49	25.61	0.73	25.09	0.85	15.56	2.78	13.02	0.36	21.64	3.87	20.66	0.97
SrO	5.95	0.74	5.01	0.61	6.27	0.68	6.77	0.79	7.01	1.59	4.52	0.58	4.51	0.23	5.18	1.69	13.70	0.74
ThO_2	0.27	0.06	0.08	0.05	0.19	0.09	0.02	0.03	0.04	0.01	0.01	0.01	0.02	0.02	0.01	0.01	0.06	0.03
As_2O_5	0.13	0.05	0.02	0.02	0.05	0.03	0.01	0.01	0.05	0.03	15.72	4.32	17.85	0.79	6.04	5.16	0.24	0.06
Total	83.97	1.17	85.56	1.25	79.85	1.57	85.86	1.46	85.19	0.74	89.04	1.16	88.34	0.22	87.07	0.96	78.75	1.90
SiO_2[c]	*6.75*	*1.47*	*0.84*	*0.35*	*8.32*	*3.91*	*0.88*	*0.30*	*0.98*	*0.17*	*0.70*	*0.59*	*0.70*	*0.22*	*0.69*	*0.58*	*9.74*	*5.57*
apfu																		
Ca	0.28		0.28		0.18		0.27		0.25		0.31		0.31		0.33		0.16	
Sr	0.28		0.23		0.31		0.31		0.32		0.18		0.22		0.24		0.68	
Nd	0.04		0.08		0.08		0.05		0.06		0.02		0.02		0.01		0.04	
Pr	0.02		0.02		0.02		0.02		0.01								0.01	
Ce	0.27		0.20		0.15		0.18		0.17		0.34		0.29		0.30		0.05	
La	0.09		0.11		0.13		0.12		0.10		0.04		0.05		0.04		0.03	
Fe^3			0.01		0.12		0.03		0.02		0.14		0.21		0.17			
Al			0.08				0.03		0.01									
Th	0.01																	
A	**0.97**		**1.01**		**0.99**		**1.00**		**0.95**		**1.03**		**1.10**		**1.09**		**0.98**	
Al	2.86		3.00		3.06		3.00		3.00		2.92		2.84		2.96		2.96	
Fe^{3+}	0.09		0.00		0.00		0.00		0.00		0.08		0.16		0.04		0.02	
B	**2.95**		**3.00**		**3.06**		**3.00**		**3.00**		**3.08**		**3.00**		**3.00**		**2.98**	
P	1.86		1.72		1.74		1.71		1.70		1.08		0.92		1.46		1.50	
S	0.21		0.27		0.20		0.28		0.35		0.18		0.18		0.19		0.54	
As	0.01										0.63		0.78		0.26		0.01	
X	**2.07**		**1.99**		**1.94**		**2.00**		**2.05**		**1.89**		**1.88**		**1.91**		**2.05**	
ΣLREE	0.41		0.41		0.38		0.36		0.35		0.40						0.13	
Ce anomaly[d]	1.59		0.89		0.57		0.86		1.02		6.00		3.25		4.42		0.65	
S/P	0.11		0.16		0.12		0.17		0.21		0.17		0.20		0.13		0.36	

brighter parts contain higher LREE.

In all samples, APS minerals commonly occur in contact and/or are spatially associated with zircon (Figs. 4f and 4g), primary apatite (Fig. 4l), or sulfide minerals, such as pyrite (Fig. 4k) and lesser chalcopyrite (Fig. 4d). Zircon grains associated with APS minerals are commonly fractured and/or partially dissolved and rimmed by xenotime (cf. Quirt et al. 1991) (Fig. 4g). Apatite forms subhedral, rounded crystals. APS minerals also occur with small hydrothermal fluorapatite crystals. APS minerals commonly contain inclusions of sulfides or Fe-oxide (Figs. 4h and 4k, 4l). APS minerals in the Zone 2 ore body are in close proximity (within the same thin section) with uraninite.

APS mineral chemistry—major elements

The APS mineral formulas were calculated based on 6 cations (Table 2) as the ideal formula is expressed as $AB_3(XO_4)_2(OH)_6$, where A = mono-, di-, tri- or, more rarely, tetravalent cations (K^+, Na^+, Rb^+, Ca^{2+}, Sr^{2+}, REE^{3+}, Th^{4+} etc.); B = Al^{3+}, Fe^{3+}; and X = P^{5+}, S^{6+}, and As^{5+}. Cation charges were allocated using the following: (1) the X-site was filled with P^{5+}, S^{6+}, As^{5+}, (2) the B-site was filled by Al^{3+}, then Fe^{3+} to have three cations, and (3) the A site was then filled by remaining cations.

High contents of trivalent cations occur in the A-site and create excess cation charges. To compensate for this, $PO_3(OH)^{2-}$ was assigned for $(PO_4)^{3-}$, as has been used by previous researchers (e.g.,

Gaboreau et al. 2007).

Along the P2 fault, APS minerals occur predominately with sudoite and lesser illite and magnesiofoitite, in intensely altered metapelite and pegmatite. These APS minerals contain high ΣLREE (0.35–0.58 apfu; LREE = La + Ce + Pr + Nd) relative to Sr (0.16–0.32 apfu) and Ca (0.18–0.28), and high PO_4^{3-} (1.70–1.97 apfu) relative to SO_4^{2-} (0.06–0.35 apfu) and AsO_4^{3-} (<0.01 apfu) (Table 2). Ce is high (0.15–0.27 apfu) relative to La (0.09–0.17 apfu), and Pr (<0.01–0.03 apfu), producing $[Ce]_N/[Ce]_N^*$ of ~0.8–1.6, where $[Ce]_N^* = \sqrt{([La]_N \cdot [Pr]_N)}$. Cores of zoned grains are enriched in Sr, Ca, and S, and rims contain high LREE and P (Fig. 5a; Table 2). Within the cores, Ca and P contents are inversely correlated with Sr and S contents (Fig. 5a). The narrow width of zoning and small size of grains prevented acquisition of quantitative compositions of individual zones excluding coarse grains in MAC152 (Table 2). Therefore, most data presented in Table 2 represents mixtures (referred to as mixed data) of compositional zones identified in SEM-BSE.

APS minerals in the sample of Bleached Zone quartzite (MAC17) contain high Sr (0.68 apfu) relative to Ca (0.16 apfu) and ΣLREE (0.13 apfu) and high SO_4^{2-} (0.54 apfu; Table 2).

APS minerals are abundant in the Red-Green Zone sample of the basement footwall (MAC412) near the P2 Main deposit. APS minerals occur with clinochlore and sudoite and contain high AsO_4^{3-} (~ 0.63 apfu), Fe^{3+} (0.16 apfu), and Ce (~0.32 apfu) show-
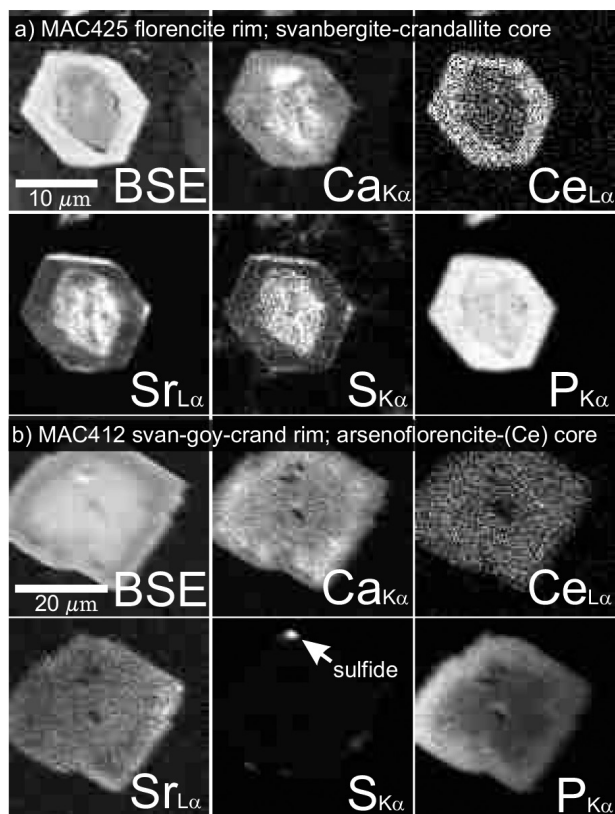
FIGURE 5. X-ray maps of APS minerals showing zoning with respect to Ca, Ce, Sr, S, and P obtained by wavelength-dispersive spectra of EPMA: (**a**) sample MAC425 from the P2 fault and Zone 2 ore body and (**b**) sample MAC412 from the Red-Green Zone (locations shown in Fig. 2; see Table 2 for quantitative chemical data). svan-goy-crand = svanbergite-goyazite-crandallite. Note that very dark areas in BSE images contain low mass elements and they are not holes or other mineral inclusions.

ing positive Ce anomalies ([Ce]/[Ce]*) of up to 6. APS minerals from this sample are also zoned with high-Ce cores, and a Ca- and P-rich inner rim and Sr-rich outer rim (Fig. 5b). APS minerals in this sample were relatively coarse grained; therefore, individual core and rims were analyzed in two grains (Table 2). The data shows that the cores contain high As (0.78 apfu) and low P (0.92 apfu) relative to the rim (0.26 and 1.46 apfu, respectively; Table 2).

APS mineral chemistry—trace elements

LA-ICP-MS analyses were conducted on relatively coarse-grained (>10 μm) APS minerals proximal to the Zone 3 (sample MAC44) and Zone 2 ore deposits (samples MAC63 and MAC85). Counts of all elements were monitored during the analysis to detect mineral inclusions and contributions of surrounding minerals. Mineral inclusions should give sharp increases in the counts of elements, but no such spikes were observed during the analysis, confirming the lack of mineral inclusions. None of surrounding minerals contain any significant concentrations of elements described below. Counts of elements, such as U, Y, Pb, and Th were at background levels in surrounding minerals and only high when the laser beam hit APS grains. Unlike clays, APS minerals

show high counts of LREE, Sr, Ca, and P (Appendix Fig. 1[1]). This confirms that these elements are in the APS crystal structure and were not incorporated from surrounding minerals. Furthermore, different grains from individual sections yielded comparable concentrations of minor and trace elements, suggesting that these trace elements originate from APS minerals and that the values are minima since the dilution effects by the surrounding minerals were not corrected. The dilution effects by surrounding minerals are confirmed by the detection of significant Si (48 000–99 000 ppm) during the ablation of the APS minerals.

APS minerals in the P2 fault proximal to Zone 3 (MAC44) ore deposit contain appreciable Se (130 ppm), U (0.39–0.88 ppm), Pb (160–180 ppm), and Th (1100–1600 ppm). Similarly, APS from sample MAC63 (~50 m) from Zone 2 ore and ~20 m into the hanging-wall of the P2 fault) show appreciable Se (100–160 ppm), U (1.7–4.2 ppm), Pb (82–190 ppm), and Th (1000–1400 ppm). Sample MAC85, from within 20 m of Zone 2 ore and directly within the P2 fault, contains APS with relatively high U (16 ppm), Pb (260 ppm), and Th (2300 ppm). Similar to samples MAC44 and MAC63, sample MAC85 showed appreciable Se (130 ppm). Combined with the EPMA data of major elements (La, Ce, Pr, Nd), these APS minerals from the P2 fault area contain high LREE relative to HREE ([LREE]$_N$/[HREE]$_N$ = 800–2500; Fig. 6) and show low S/Se weight ratios, ranging from 100–150.

DISCUSSION

Major element compositions of APS minerals

The following elemental relationships are observed:

(1) The P contents positively correlate with LREE and both inversely correlate with Sr and S (Figs. 5a,7c, and 7d). The LREE inversely correlate with Ca (Figs. 5a and 7e).

(2) The S contents positively correlate with Sr and inversely correlate with Ce (Figs. 5a and 7b).

(3) High Ca correlates with high P (Figs. 5a and 5b).

(4) The As contents inversely correlate with P (Fig. 7a).

(5) High As APS minerals contain high Ce relative to other REE (Fig. 7a).

The above relationships and cations in A-site and X-site suggest the presence of the following end-members (Fig. 8):

High LREE and P contents correspond to high proportions of florencite (REE)Al$_3$(PO$_4$)$_2$(OH)$_6$ (Figs. 8a–8c). High S and Sr contents correspond to high proportions of svanbergite SrAl$_3$(PO$_4$)(SO$_4$)(OH)$_6$ with a minor goyazite component SrAl$_3$(PO$_4$)$_2$(OH)$_6$ (Figs. 8a–8d).

High Ca contents correspond to high proportions of crandallite CaAl$_3$(PO$_4$)$_2$(OH)$_6$ (Figs. 8a, 8b, and 8d).

High As and high Ce contents correspond to high proportions of arsenoflorencite-(Ce) (Ce,REE)Al$_3$(AsO$_4$)$_2$(OH)$_6$ (Figs. 8a and 8b).

APS minerals show wide compositional variations, but all can be expressed using the above five end-members (crandallite, goyazite, svanbergite, florencite, and arsenoflorencite).

Spatial, chemical, and temporal variation of APS minerals and associated clay minerals

Along the entire studied range of the P2 fault, APS minerals occur with sudoite (± illite, magnesiofoitite) in metapelite and
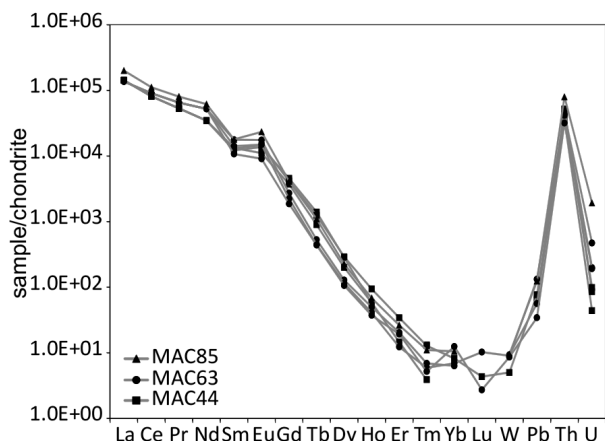
FIGURE 6. Chondrite-normalized REE, U, Th, Pb, and W for APS grains from sample MAC44 (along the P2 fault proximal to the Zone 3 ore body of the McArthur River deposit) and from samples MAC63 and MAC85 (close to Zone 2 ore). The abundance of these elements was obtained using EPMA (La, Ce, Pr, and Nd) and LA-ICP-MS (Sm, Eu, Gd, Tb, Dy, Ho, Er, Tm, Yb, Lu, W, Pb, Th, and U). Error bars are not shown in the diagram because the uncertainty of the analysis (<10%) is smaller than the size of symbols. Sample locations are in Figure 2 and Table 1. Each line represents one APS grain. Chondrite values from McDonough and Sun (1995).

pegmatite. The APS minerals are florencitic, but contain significant Ca, Sr, and SO_4^{2-} reflecting a minor component of svanbergite, mainly as core (Figs. 5a and 9).

Gaboreau et al. (2005, 2007) found that APS minerals proximal to uranium deposits contain high LREE and P relative to those in intermediate and distal areas (Fig. 9). The present study found a large compositional variation of APS minerals even within the ore, compared to the narrow range presented by Gaboreau et al. (2005, 2007), and the compositional variation does not correlate with distance from uranium mineralization (Fig. 9). For example, the (LREE+P)/(Ca+Sr+S) ratios of APS minerals near (<1 m) the uranium ore range from 1.6 to 5.6, whereas those from barren samples far (>500 m) from mineralization vary from 2.8–4 (Fig. 9). We suggest that our data reflects the evolution of fluids in the ore zone where the earlier fluids contained high in Ca, Sr, and SO_4^{2-}, and evolved to have high LREE and P. This proposed interpretation is supported by compositional zoning of APS minerals with Ca-, Sr-, and S-rich cores and LREE- and P-rich rims (Fig. 5a).

APS minerals are abundant with kaolin and illite in one sample of the Bleached Zone (MAC17) along the unconformity. These grains are Sr- and S-rich and similar in composition within the sample but not with the APS minerals found along the P2 fault (Fig. 9). The average composition of the APS minerals is $Ca_{0.16}Sr_{0.68}Ce_{0.05}La_{0.03}Nd_{0.04}Pr_{0.01})(Al_{2.96}Fe_{0.02}^{3+})(PO_3O_{0.94}OH_{0.06})_{1.50}$ $(SO_4)_{0.54}(AsO_4)_{0.01}(OH)_6$, svanbergite$_{0.54}$-crandallite$_{0.16}$-goyazite$_{0.14}$-florencite$_{0.13}$. The data are comparable to APS mineral compositions in distal sandstones by Gaboreau et al. (2007) (Fig. 9).

One Red-Green Zone sample of intensely altered metapelite (MAC412) footwall to the P2 fault, contain APS minerals with As- and Ce-rich cores and Ca-, Sr-, and S-rich rims together with clinochlore and sudoite. The grains show similar Ca, Sr, and S contents

with varying LREE and P due to the presence of As that substitutes for P (Figs. 7a and 9). The average composition of these grains is $(Ca_{0.31}Sr_{0.22}Ce_{0.32}La_{0.04}Nd_{0.02}Fe_{0.15})(Al_{2.92}^{3+}Fe_{0.08})(PO_3O_{0.83}OH_{0.17})_{1.11}$ $(SO_4)_{0.18}(AsO_4)_{0.68}(OH)_6$, arsenoflorencite(-Ce)$_{0.39}$-crandallite$_{0.31}$-svanbergite$_{0.18}$-goyazite$_{0.12}$. This is the first documented occurrence of arsenoflorencite(-Ce) in the Athabasca Basin.

APS minerals from the McArthur River deposit and the P2 fault show cores of svanbergite-crandallite-goyazite rimmed by florencite (Figs. 4c–4e, 4k, 4l, and 5a). APS minerals from the Red-Green Zone contain arsenoflorencite-(Ce) cores rimmed by svanbergite-crandallite-goyazite (Figs. 4h, 5b, 8b). APS minerals of the Bleached Zone are svanbergite-crandallite-goyazite (Fig. 8). The zoning suggests the crystallization sequence of APS minerals in the study area. Early crystallization of arsenoflorencite (Ce) was followed by svanbergite-crandallite-goyazite, and finally florencite.

Nature of fluids responsible for APS mineral formation

APS minerals in the Bleached Zone sample contain high SO_4^{2-} contents, up to 0.59 apfu (Figs. 7b and 7d, 8b–8d), indicating relatively oxidizing conditions for their formation. These APS minerals have close to svanbergite end-member composition with a minor goyazite and crandallite component (Figs. 7b and 7d–7e; 8, 10). The grains coexist with kaolin and illite (Fig. 4i), which is the diagenetic assemblage in the Athabasca Group sandstones (Hoeve and Quirt 1984; Quirt 2001). The composition of the APS minerals is similar to those of diagenetic origin reported in Athabasca and Kombolgie sandstones (Gaboreau et al. 2005, 2007), and other sedimentary basins worldwide (Spötl 1990; Gaboreau et al. 2005, 2007; Pe-Piper and Dolansky 2005; Gall and Donaldson 2006; Fig. 10). Therefore, the APS minerals of the Bleached Zone along the unconformity most likely crystallized from an oxidizing, Ca-, Sr- and SO₄-rich, diagenetic fluid of the overlying sandstones.

The oxidizing conditions of diagenetic fluids from the sandstones are recorded as relict cores of the APS minerals along the P2 fault in the basement (Figs. 4 and 5a). These cores contain high Ca, Sr, and S and are similar in composition to diagenetic APS minerals in sandstones described above. The S/P ratios of APS minerals as whole grains along the P2 fault are relatively low (<0.16) compared to those of the Bleached Zone (0.36; Table 2). The lowest S/P ratios (<0.06) are found in areas of Zone 2 ore (Fig. 11b). The data shows that the SO_4^{2-} contents in fluids decreased from the unconformity to the P2 fault and from non-mineralized areas along the P2 fault to ore zone. This indicates the change from a relatively oxidized to a relatively reduced environment. This modification of fluid chemistry may have taken place due to interaction of fluids with graphite-rich basement rocks, as has been suggested by Gaboreau et al. (2007). Alternatively, it was caused by reduced fluids that originated from the graphite-rich basement rocks and supplied through faults. In either case, this redox change closer to the uranium ore is consistent with the reduction of U^{6+} to U^{4+} necessary for the precipitation of uraninite. Therefore, S/P ratios of APS minerals record the reduction of fluids associated with uranium mineralization.

The spatial association of florencitic APS minerals with the McArthur River uranium deposit (Fig. 2b) and their abundance within the deposit suggest the close relationship between
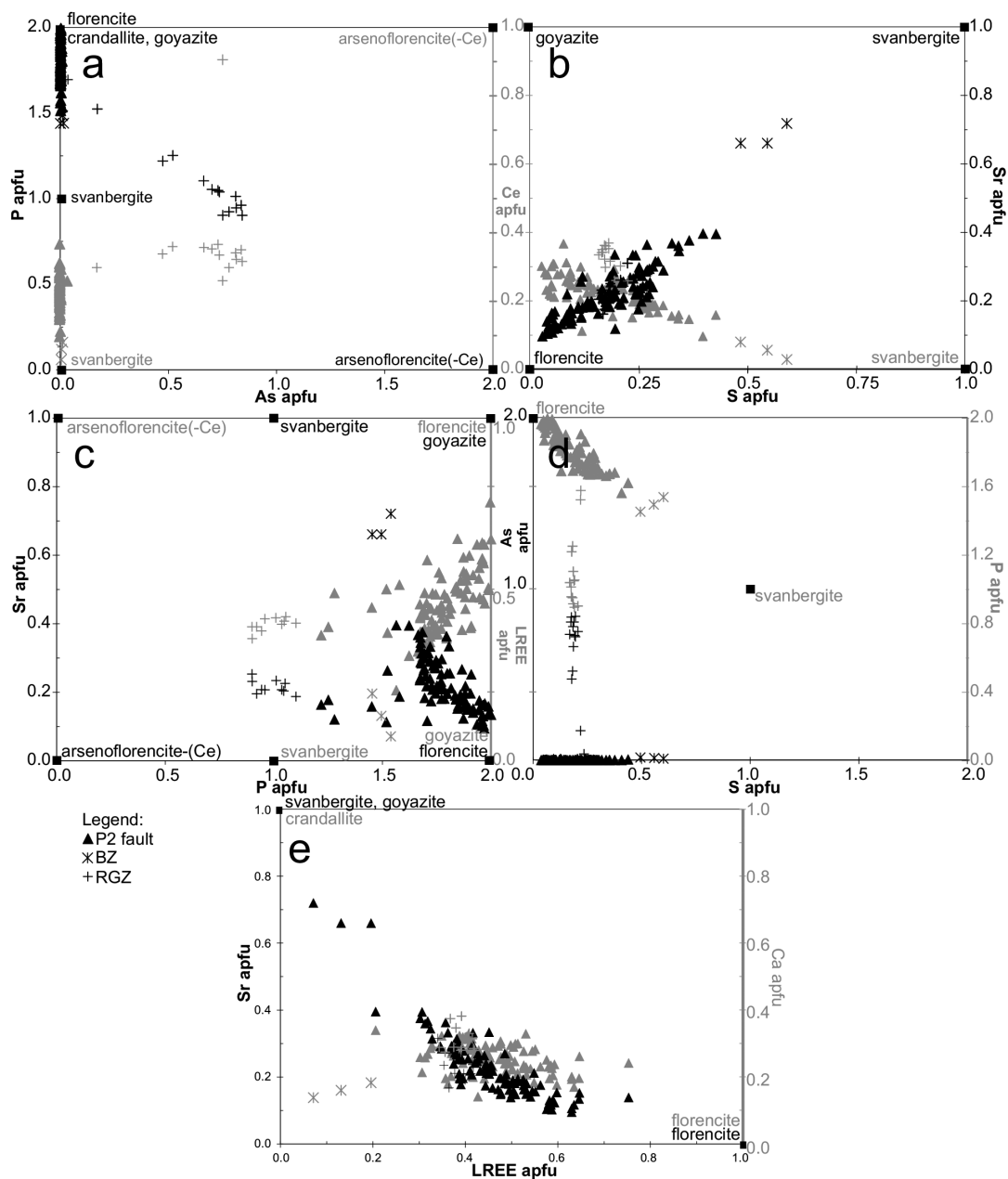
FIGURE 7. Binary plots showing substitution and elemental relationships of APS minerals based on EPMA data: (**a**) As vs. P (black) and As vs. Ce (gray); (**b**) S vs. Sr (black) and S vs. Ce (gray); (**c**) P vs. Sr (black) and P vs. LREE (gray); (**d**) S vs. As (black) and S vs. P (gray); and (**e**) LREE vs. Sr (black) and LREE vs. Ca (gray). Each data point represents one grain. P2 fault = P2 fault samples (triangles). BZ = Bleached Zone sample (stars). RGZ = Red-Green Zone sample (crosses).

florencite and the uranium mineralization. This observation is consistent with that of Gaboreau et al. (2007). The APS minerals in metapelite and pegmatite along the entire 7 km of the P2 fault studied are predominantly florencite with minor components of svanbergite-crandallite-goyazite (Figs. 4d–4e, 9). The alteration assemblage of sudoite, magnesiofoitite, and illite is also similar all along the P2 fault including the ore zone. The evidence suggests that similar fluids passed along the entire P2 fault. These fluids were likely uranium-bearing because APS minerals contain uranium (up to 16 ppm; Table 3).

The Red-Green Zone sample of metapelite (sample MAC412; Fig. 3d) contains As- and LREE-rich APS minerals (Figs. 7a and 7d; Table 2). Arsenic in APS minerals occur as As^{5+}, replacing P^{5+} in the X-site of the crystal structure. These As-bearing crystals show prominent zoning with cores of arsenoflorencite-(Ce) and rims of crandallite-goyazite and svanbergite solid-solution (Figs. 5b, 7a, 7c, 8b; Table 2) with sharp boundaries. The zoning suggests that arsenoflorencite-(Ce) formed earlier than the svanbergite-crandallite-goyazite of diagenetic origin. This arsenoflorencite-(Ce) may have formed in the very early stage
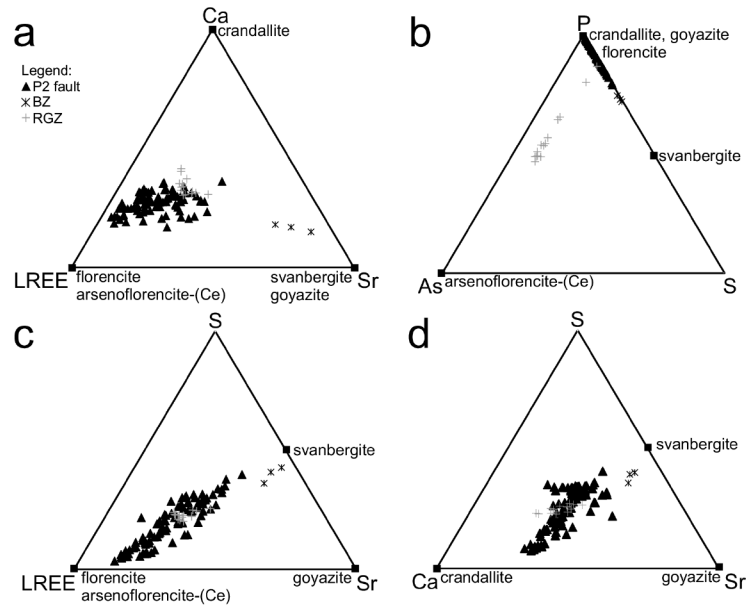
FIGURE 8. Compositions of APS minerals plotted on ternary diagrams. End-member minerals are indicated. (**a**) Ca-Sr-LREE; (**b**) P-S-As; (**c**) S-Sr-LREE; (**d**) S-Sr-Ca. Each data point represents one grain. P2 fault = P2 fault samples (triangles). BZ = Bleached Zone sample (stars). RGZ = Red-Green Zone sample (crosses).
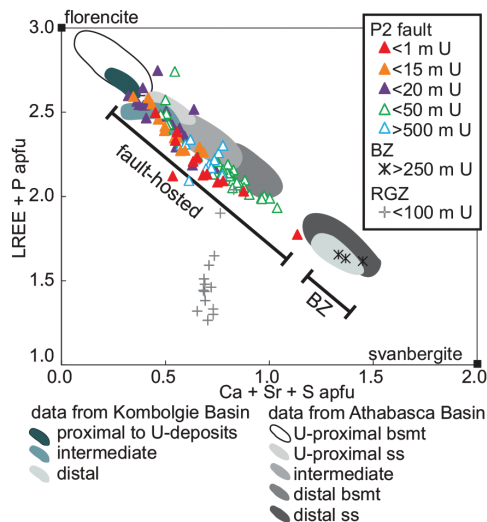
FIGURE 9. Cross-plot showing coupled substitution of Ca-Sr-S for LREE-P for APS minerals along the P2 fault (triangles), and within the Bleached Zone (BZ) (stars) and Red-Green Zone (RGZ) (crosses). P2 fault samples are color coded with respect to distance in meter from uranium mineralization (McArthur River deposit and low-grade): red filled triangles represents sample <1 m from ore (MAC425 and MAC29), orange filled triangles were <15 m from ore (MAC152), purple filled triangles were <20 m from ore (MAC67 and MAC85), open green triangles were <50 m from ore (MAC43, MAC44, MAC63, and MAC404), and open blue triangles were of unmineralized areas >500 m from the ore (MAC117 and MAC135). Each data point represents one grain. For comparison, the diagram shows the compositional ranges of APS minerals determined by Gaboreau et al. (2005, 2007) from the Athabasca Basin (fields with various shades of gray) and Kombolgie Basin, Australia (field with various shades of blue). (Color online.)
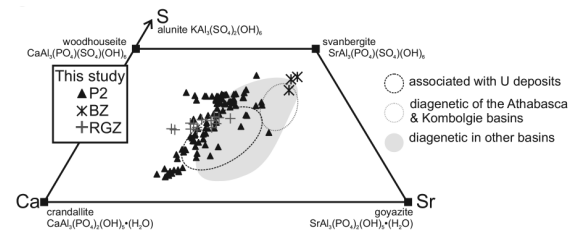
FIGURE 10. An alunite-goyazite-crandallite [S-Sr-Ca] ternary plot showing compositions of APS minerals from the P2 fault (P2; triangles), the Bleached Zone (BZ; stars), and the Red-Green Zone (RGZ; crosses). Each data point represents one grain. For comparison, the compositional ranges of diagenetic APS minerals from various sedimentary units are shown: diagenetic APS minerals of the Athabasca and Kombolgie basins are represented by gray dotted field (Gaboreau et al. 2005, 2007) and diagenetic APS minerals of the Chaswood Formation (Pe-Piper and Dolansky 2005), Hornby Basin and Thelon Basins (Gall and Donaldson 2006), and Mitterberg Formation (Spötl 1990) are collectively represented by the gray field. APS minerals associated with uranium deposits of the Athabasca and Kombolgie Basin (Gaboreau et al. 2005, 2007) are represented by the black dashed field.

of diagenesis. If this is the case, As-rich APS minerals should be observed in sandstones. However, there is no record of As-rich APS minerals in the Athabasca sandstone. Furthermore, sharp boundaries between cores and with rims suggests that As-rich APS minerals formed before the sandstone diagenesis. We suggest that, arsenoflorencite(-Ce) cores may have formed during paleo-weathering before the deposition of the Athabasca sandstones. This proposed interpretation is further supported by the presence of As^{5+} in the APS minerals. Although As contents are high in organic-rich shale (e.g., Ketris and Yudovich 2009), As
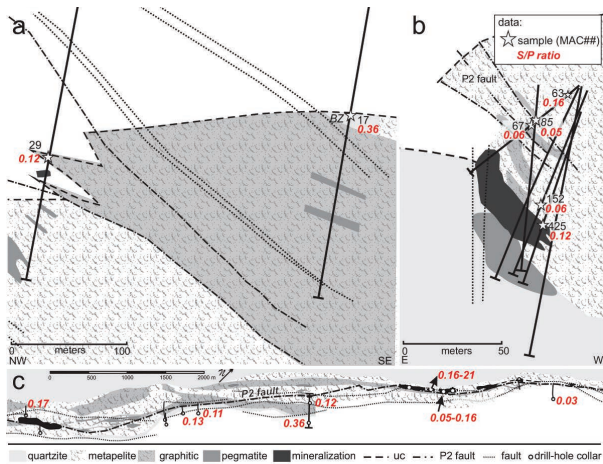
FIGURE 11. Spatial variation of S/P ratios for APS minerals. The average S/P ratio (mixed data, see Table 2) of APS minerals within a sample is expressed as a red, bold, italicized number next to its corresponding sample (**a** and **b**) or drill-core (**c**) location. (Color online.)

TABLE 3. LA-ICPMS data of APS (ppm)

Sample:	44		63		85	BCR2G[a]	1σ	Precision	Accuracy[b]
No. grains	3	1σ	3	1σ	1			%	%
Li	150	19	190	16	150	9	0.97	1.3	0.78
Si	48000	12000	68000	12000	99000	247000	3900	1.11	2.5
Ca	15000	1000	13000	3000	18000	48000	540	1.2	6.8
Sc	8.1	1.7	4.9	0.80	<3	28	0.35	0.46	14
Ti	31	17	26	5.5	52	12000	83	1.13	13
V	20	10	20	7.5	13	400	1.43	1.08	4.7
Cr	31	12	16	3.6	<30	15	0.29	0.50	18
Mn	30	7.6	18	5.8	55	1560	2.11	0.27	2.9
Fe	7600	1600	6300	3100	3500	85000	1300	1.48	12
Co	4.0	0.42	70	96	3.7	36	0.05	0.46	2.4
Ni	21.43	1.21	49	43	<10	10	0.82	1.07	
Cu	5.4	0.53	5.7	0.79	72	16	0.12	0.67	16
Zn	4.4	0.19	9.0	4.7	<8	150	1.4	1.56	15
Se	130	2.6	120	20	130	< 3		1.85	
Rb	17	11	2.0	0.23	5.0	46	0.45	0.40	4.9
Sr	42000	7000	23000	6300	24000	310	2.7	0.79	10
Y	57	7.6	38	2.7	60	28	0.025	1.16	23
Zr	1.1	0.66	7.0	2.1	7.1	160	0.87	0.35	17
Nb	0.28	0.16	0.15	0.04	<0.3	10	0.01	0.53	
Mo	3.4	1.3	8.3	9.5	<4	240	0.86	1.06	3.1
Sn	2.3	0.86	3.3	1.2	2	2	0.03	1.08	
Ba	630	63	250	74	440	620	9.6	0.72	9.9
La	20000	3500	24000	5300	34200	23	0.25	1.36	6.3
Ce	39000	8000	45000	9400	58000	50	0.97	0.70	11
Pr	3800	500	4600	840	5900	5.8	0.035	0.75	15
Nd	14000	1400	17000	3200	20400	26.0	0.74	1.21	7.3
Sm	2000	69	2200	440	2800	5.7	0.17	0.68	14
Eu	760	87	800	200	1300	1.8	0.059	0.67	9.0
Gd	820	68	450	69	810	6.0	0.42	1.05	11
Tb	43	7.6	17	1.5	40	0.9	0.012	1.28	15
Dy	64	10	28.63	2.3	60	6	0.01	0.99	
Ho	3.8	0.94	2.3	0.29	3.7	1.2	0.010	0.84	10
Er	2.9	1.9	2.8	0.58	4	3	0.095	1.24	
Tm	0.25	0.11	0.148	0.017	0.27	0.40	0.02	1.37	28
Yb	0.94	0.34	1.4	0.45	1.7	2.8	0.21	0.77	18
Lu	0.13	0.033	0.14	0.081		0.41	0.032	0.75	20
Hf	0.91	0.40	0.30	0.099	<0.53	4.3	0.23	1.32	11
Ta	0.17	0.10	0.077	0.08	<0.161	0.6	0.007	1.56	
W	0.79	0.36	0.9	0.029	1	0.5	0.03	0.61	
Pb	160	10	120	39	260	10.3	0.005	0.92	12
Th	1300	200	1100	140	2300	5.4	0.035	0.91	13
U	0.62	0.19	2.4	1.1	16	1.7	0.065	1.46	1.9

Note: Data is the average of anaylzed grains (no. grains) in the sample (±1 st.dev.).
[a] BCR2G from U.S. Geological Survey.
[b] Based on the data of BCR2G provided by USGS.

is mostly fixed in sulfide minerals (e.g., Ryan et al. 2013). For As to be incorporated in the APS minerals, it must be oxidized to As^{5+}, which is stable in oxidizing, near-surface conditions (Smedley and Kinniburgh 2002).

APS minerals related to uranium deposits and role of P2 fault

It has been suggested that APS minerals with florencitic compositions are contemporaneous with uranium mineralization based on their occurrences within uranium deposits (Quirt et al. 1991; Gaboreau et al. 2005, 2007; Mercadier et al. 2011). Here we have shown that APS minerals of florencitic composition are found along a 7 km strike length of the P2 fault, even in areas barren of mineralization (Table 2; Fig. 9); although, as previously discussed, APS minerals with the highest florencite component (reflecting relatively reducing conditions) are found in proximity to ore (Figs. 9 and 11). The APS minerals also contain elevated uranium contents (Table 3; Fig. 6), suggesting that florencitic APS minerals crystallized from uranium-bearing fluids that became reduced. The evidence supports that florencite was contemporaneous with uranium mineralization.

Florencitic APS minerals are not found in the basement greater than ~50 m from the center of the P2 fault (Table 1; Fig. 9). The distribution of the APS minerals constrains the extent of the fluid footprint, and suggests that the entire P2 fault was a conduit for an oxidizing uranium-bearing fluid during mineralization. The P2 fault was also a site of redox change where an initial oxidizing fluid became modified and relatively reducing.

IMPLICATIONS

APS minerals are very small in size, but ubiquitous in the altered metasedimentary rocks along the P2 fault, which hosts the McArthur River uranium deposit. Previous researchers noted the spatial association of florencitic APS minerals and uranium deposits and suggested their use as an exploration vector (e.g., Gaboreau et al. 2007). Our study reveals that APS minerals record the timing and characteristics of geological events, from paleo-weathering, diagenesis to uraniferous hydrothermal activity. We conclude that oxidizing diagenetic fluids traveled along P2 fault and formed svanbergite-crandallite-goyazite. The fluid evolved to become reducing through interaction with the basement rocks and formed florencite rims. Our study shows that APS minerals are an excellent mineralogical tool to fingerprint fluid pathways. APS minerals with similar chemistry (high florencite component) are found along a 7 km of strike length of the P2 fault, including areas barren of uranium mineralization. This suggests that uranium-bearing fluids likely passed along the entire P2 fault, but only produced uranium mineralization in localized areas. This study confirms that APS minerals are good indicators of alteration related to uranium mineralization, thus they may be useful to identify fertile structures associated with uranium deposits.

REFERENCES CITED

Adlakha, E.E., Hattori, K., Zaluski, G., Kotzer, T., and Potter, E.G. (2014) Alteration within the basement rocks associated with the P2 fault and the McArthur River uranium deposit, Athabasca Basin. Geological Survey of Canada Open File 7462, 35 p., http://dx.doi.org/10.4095/293364.

Alexandre, P., Kyser, K., Polito, P., and Thomas, D. (2005) Alteration mineralogy and stable isotope geochemistry of Paleoproterozoic basement-hosted unconformity-type uranium deposits in the Athabasca Basin, Canada. Economic Geology, 100, 1547–1563.

Alexandre, P., Kyser, K., Jiricka, D., and Witt, G. (2012) Formation and evolution of the Centennial unconformity-related uranium deposit in the South-Central Athabasca Basin, Canada. Economic Geology, 107, 385–400.

Annesley, I.R., Madore, C., and Portella, P. (2005) Geology and thermotectonic evolution of the western margin of the Trans-Hudson Orogen: Evidence from the eastern sub-Athabasca basement, Saskatchewan. Canadian Journal of Earth Sciences, 42, 573–597.

Beaufort, D., Patrier, P., Laverret, E., Bruneton, P., and Mondy, J. (2005) Clay alteration associated with Proterozoic unconformity-type uranium deposits in the East Alligator Rivers uranium field, Northern Territory, Australia. Economic Geology, 100, 515–536.

Bronkhorst, D., Mainville, A.G., Murdock, G.M., and Yesnik, L.D. (2012) McArthur River Operation Northern Saskatchewan, Canada: National Instrument 43-101 Technical Report.

Cuney, M., Brouand, M., Cathelineau, M., Derome, D., Freiberger, R., Hecht, L., Kister, P., Lobaev, V., Lorilleux, G., Peiffert, C., and Bastoul, A.M. (2003) What parameters control the high grade–large tonnage of the Proterozoic unconformity related uranium deposits? In M. Cuney, Ed., Uranium Geochemistry 2003, International Conference, April 13–16, 2003, p. 123–126. Proceedings: Unité Mixte de Recherche CNRS 7566 G2R, Université Henri Poincaré, Nancy, France.

Derome, D., Cathelineau, M., Cuney, M., Fabre, C., Lhomme, T., and Banks, D.A. (2005) Mixing of sodic and calcic brines and uranium deposition at McArthur River, Saskatchewan, Canada: A Raman and laser-induced breakdown spectroscopic study of fluid inclusions. Economic Geology, 100, 1529–1545.

Dill, H.G. (2001) The geology of aluminium phosphates and sulfates of the alunite group minerals: A review. Earth-Science Reviews, 53, 35–93.

Gaboreau, S., Beaufort, D., Vieillard, P., Patrier, P., and Bruneton, P. (2005) Aluminum phosphate–sulfate minerals associated with Proterozoic unconformity-type uranium deposits in the East Alligator River Uranium Field, Northern Territories, Australia. Canadian Mineralogist, 43, 813–827.

Gaboreau, S., Cuney, M., Quirt, D., Beaufort, D., Patrier, P., and Mathieu, R. (2007) Significance of aluminum phosphate-sulfate minerals associated with U unconformity-type deposits: The Athabasca Basin, Canada. American Mineralogist, 92, 267–280.

Gall, Q., and Donaldson, J.A. (2006) Diagenetic fluorapatite and aluminum phosphate sulfate in the Paleoproterozoic Thelon Formation and Hornby Bay Group, northwestern Canadian Shield. Canadian Journal of Earth Sciences, 43, 617–629.

Hajnal, Z., White, D.J., Takacs, E., Gyorfi, I., Annesley, I.R., Wood, G., and Nimeck, G. (2010) Application of modern 2-D and 3-D seismic-reflection techniques for uranium exploration in the Athabasca Basin. Canadian Journal of Earth Sciences, 47, 761–782.

Hoeve, J., and Quirt, D.H. (1984) Mineralization and host-rock alteration in relation to clay mineral diagenesis and evolution of the Middle Proterozoic Athabasca Basin, Northern Saskatchewan, Canada. Saskatchewan Research Council, Technical Report 189, 189 p.

Hoeve, J., and Sibbald, T.I. (1978) On the genesis of Rabbit Lake and other unconformity-type uranium deposits in northern Saskatchewan, Canada. Economic Geology, 73, 1450–1473.

Hoeve, J., Rawsthorne, K., and Quirt, D. (1981) Uranium metallogenetic studies: Collins Bay B Zone, II. Clay mineralogy. In: Summary of Investigations 1981, Saskatchewan Geological Survey, Miscellaneous Report 81, 73–76.

Jambor, J.L. (1999) Nomenclature of the alunite supergroup. The Canadian Mineralogist, 37, 1323–1341.

Jefferson, C.W., Thomas, D.J., Gandhi, S.S., Ramaekers, P., Delaney, G., Brisbin, D., Cutts, C., Portella, P., and Olson, R.A. (2007) Unconformity-associated uranium deposits of the Athabasca basin, Saskatchewan and Alberta; in EXTECH IV: Geology and Uranium EXploration TECHnology of the Proterozoic Athabasca Basin, Saskatchewan and Alberta, Geological Survey of Canada Bulletin, 588, 23–67.

Ketris, M.P., and Yudovich, Y.E. (2009) Estimations of Clarkes for carbonaceous biolithes: World averages for trace element contents in black shales and coals. International Journal of Coal Geology, 78, 135–148.

Laverret, E., Mas, P.P., Beaufort, D., Kister, P., Quirt, D., Bruneton, P., and Clauer, N. (2006) Mineralogy and geochemistry of the host-rock alterations associated with the Shea Creek unconformity-type uranium deposits (Athabasca Basin, Saskatchewan, Canada). Part 1. Spatial variation of illite properties. Clays and Clay Minerals, 54, 275–294.

Lewry, J.F., and Sibbald, T. (1980) Thermotectonic evolution of the Churchill province in northern Saskatchewan. Tectonophysics, 68, 45–82.

Longerich, H.P., Jackson, S.E., and Günther, D. (1996) Inter-laboratory note. Laser ablation inductively coupled plasma mass spectrometric transient signal data acquisition and analyte concentration calculation. Journal of Analytical Atomic Spectrometry, 11, 899–904.

Macdonald, C. (1985) Mineralogy and geochemistry of the sub-Athabasca regolith near Wollaston Lake. Geology of Uranium Deposits: Canadian Institute of Mining and Metallurgy Special, 32, 155–158.

McDonough, W.F., and Sun, S.S. (1995) The composition of the Earth. Chemical Geology, 120, 223–253.

McGill, B., Marlatt, J., Matthews, R., Sopuck, V., Homeniuk, L., and Hubregtse, J. (1993) The P2 North uranium deposit, Saskatchewan, Canada. Exploration and Mining Geology, 2, 321–333.

McKechnie, C.L., Annesley, I.R., and Ansdell, K.M. (2012) Medium-to low-pressure pelitic gneisses of Fraser Lakes Zone B, Wollaston Domain, northern Saskatchewan, Canada: mineral compositions, metamorphic P–T–t path, and implications for the genesis of radioactive abyssal granitic pegmatites. Canadian Mineralogist, 50, 1669–1694.

Mercadier, J., Cuney, M., Cathelineau, M., and Lacorde, M. (2011) U redox fronts and kaolinisation in basement-hosted unconformity-related U ores of the Athabasca Basin (Canada): Late U remobilisation by meteoric fluids. Mineralium Deposita, 46, 105–135.

Mercadier, J., Richard, A., and Cathelineau, M. (2012) Boron-and magnesium-rich marine brines at the origin of giant unconformity-related uranium deposits: δ^{11}B evidence from Mg-tourmalines. Geology, 40, 231–234.

Quirt, D.H. (2001) Kaolinite and dickite in the Athabasca Sandstone, Northern Saskatchewan, Canada. Saskatchewan Research Council, Publication No. 10400-16D01.

Quirt, D., Kotzer, T., and Kyser, T.K. (1991) Tourmaline, phosphate minerals, zircon and pitchblende in the Athabasca Group: Maw Zone and McArthur River areas. Saskatchewan. Summary of Investigations 1991, Saskatchewan Geological Survey Miscellaneous Report, 91-4, 11.

Pe-Piper, G., and Dolansky, L.M. (2005) Early diagenetic origin of Al phosphate-sulfate minerals (woodhouseite and crandallite series) in terrestrial sandstones, Nova Scotia, Canada. American Mineralogist, 90, 1434–1441.

Ramaekers, P., Jefferson, C.W., Yeo, G.M., Collier, B., Long, D.G.F., Drever, G., McHardy, S., Jiricka, D., Cutts, C., Wheatley, K., Catuneau, O., Bernier, S., Kupsch, B., and Post, R.T. (2007) Revised geological map and stratigraphy of the Athabasca Group, Saskatchewan and Alberta; in EXTECH IV: Geology and Uranium EXploration TECHnology of the Proterozoic Athabasca Basin, Saskatchewan and Alberta. Geological Survey of Canada Bulletin, 588, 155–192.

Richard, A., Banks, D.A., Mercadier, J., Boiron, M.C., Cuney, M., and Cathelineau, M. (2011) An evaporated seawater origin for the ore-forming brines in unconformity-related uranium deposits (Athabasca Basin, Canada): Cl/Br and δ^{37}Cl analysis of fluid inclusions. Geochimica et Cosmochimica Acta, 75, 2792–2810.

Riegler, T., Lescuyer, J.L., Wollenberg, P., Quirt, D., and Beaufort, D. (2014) Alteration related to uranium deposits in the Kiggavik–Andrew Lake structural trend, Nunavut, Canada: New insights from petrography and clay mineralogy. The Canadian Mineralogist, 52, 27–45.

Ryan, P., Kim, J., Hattori, K., and Thompson, A. (2013) Dissolved arsenic in a fractured slate aquifer system, northern Appalachians, USA: Influence of bedrock geochemistry, groundwater flow paths, redox and ion exchange. Applied Geochemistry, 39, 181–192.

Smedley, P.L., and Kinniburgh, D.G. (2002) A review of the source, behaviour and distribution of arsenic in natural waters. Applied Geochemistry, 17, 517–568.

Spötl, C. (1990) Authigenic aluminium phosphate-sulfates in sandstones of the Mitterberg Formation, Northern Calcareous Alps, Austria. Sedimentology, 37, 837–845.

Stoffregen, R.E., Alpers, C.N., and Jambor, J.L. (2000) Alunite-jarosite crystallography, thermodynamics, and geochronology. Reviews in Mineralogy and Geochemistry, 40, 453–479.

Appendix Figure 1
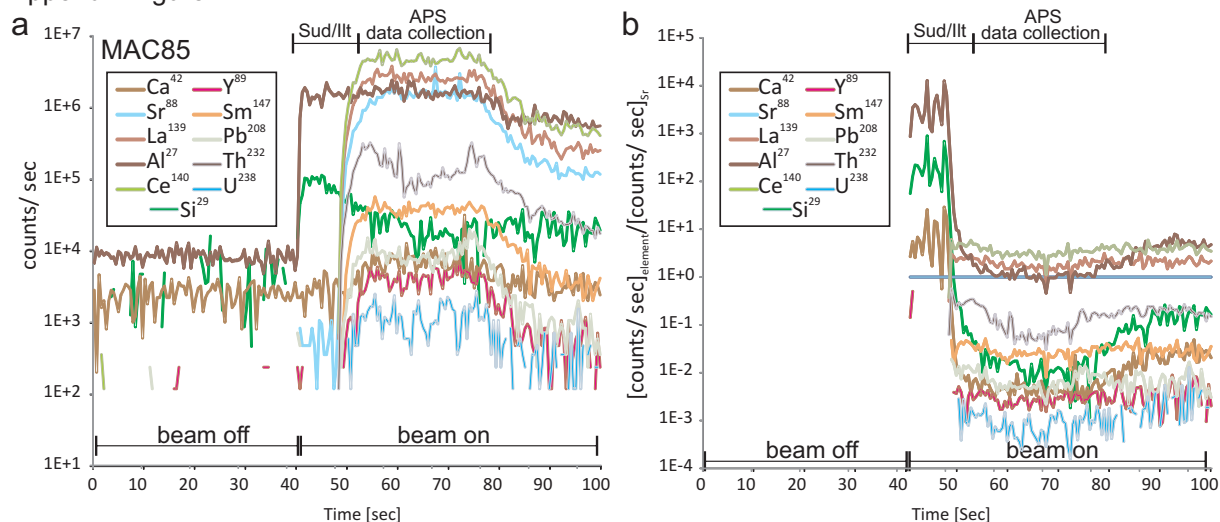
FIGURE 1. (**a**) A graph of the LA-ICP-MS analysis of an APS grain from sample MAC85 showing element counts (major and trace) vs. time in seconds. High counts of Y, Th and U correlate with high counts of the major elements in APS minerals (eg., Ce, La, Al, and Sr). This graph clearly shows that trace elements (such as Y, Th and U) are incorporated in the APS crystal structure and were not present as inclusions or contributed by surrounding minerals of sudoite (Sud) or illite (Ilt). (**b**) The same graph as shown in (**a**) but counts/s of each element is normalized to that of Sr.

Appendix Figure 2
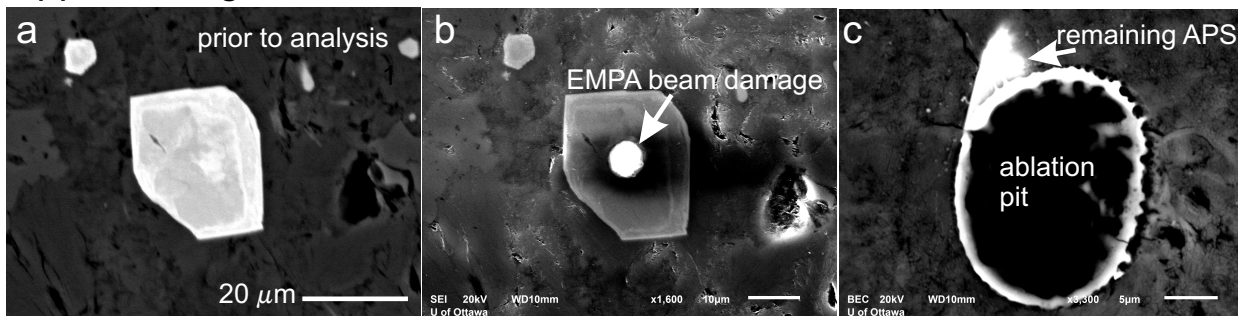
FIGURE 2. An APS mineral **(a)** before EMPA analysis and **(b)** after analysis showing beam damage. **(c)** A laser pit after LA ICP-MS analysis. **(a)** and **(c)** are BSE images and **(b)** is a secondary electron image.

Appendix Figure 3
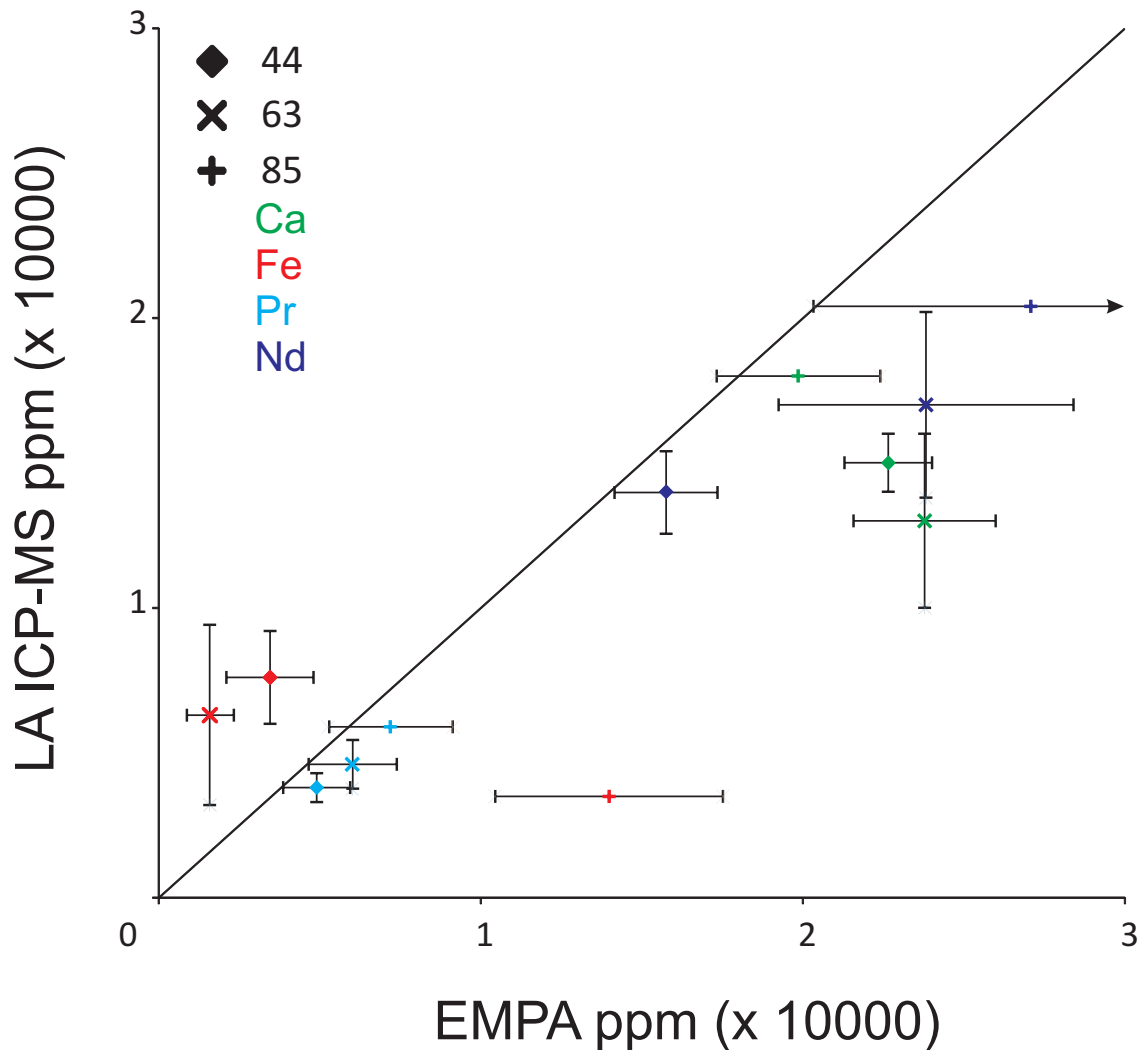
FIGURE 3. A binary plot comparing the average concentrations of Ca (green), Fe (red), Pr (cyan), and Nd (blue) in APS mineral grains from samples MAC44 (diamonds), MAC63 (**x**), and MAC85 (crosses) obtained with EMPA (Table 2) and LA ICP-MS (Table 3). Horizontal and vertical bars represent one standard deviation of the data (Tables 2 and 3). LA ICP-MS data of sample MAC85 is of one grain.